Composites Science and Technology 261 (2025) 110995

Contents lists available at ScienceDirect

Composites Science and Technology

journal homepage: www.elsevier.com/locate/compscitech

The shape effect: Influence of 1D and 2D boron nitride nanostructures on the radiation shielding, thermal, and damping properties of high-temperature epoxy composites

Kazue Orikasa [a], Luiza Benedetti [a], Sang-Hyon Chu [b], Tyler Dolmetsch [a], Alberto Jimenez [c], Denny John [a], Teagan Smith [d], Tony Thomas [a], Benjamin Boesl [a], Cheol Park [b], Arvind Agarwal [a,*]

[a] Mechanical and Materials Engineering Department, Florida International University, Miami, FL, 33174, USA
[b] Advanced Materials and Processing Branch, NASA Langley Research Center, Hampton, VA, 23681, USA
[c] Materials Science and Engineering Area, ESCET, Rey Juan Carlos University, C/Tulipán S/n, 28933, Móstoles, Madrid, Spain
[d] Biomedical Engineering Department, Case Western Reserve University, Cleveland, OH, 44106, USA

ARTICLE INFO

Keywords:
Boron nitride nanotubes
Boron nitride nanoplatelets
Neutron radiation shielding
Thermal management
Mechanical reinforcement
Freeze-drying

ABSTRACT

In space exploration, lightweight multifunctional materials capable of shielding neutron radiation, dissipating heat, and providing damping are essential. Polymer composites reinforced with boron nitride (BN) nanomaterials—specifically one-dimensional boron nitride nanotubes (BNNTs) and two-dimensional boron nitride nanoplatelets (BNNPs)—offer promising solutions. This study investigates how BN nanomaterial morphology influences the performance of high-temperature (HT) epoxy composites. We developed ultralightweight, three-dimensional BN foams comprising 1D BNNTs, 2D BNNPs, and hybrid 1D BNNT/2D BNNP structures *via* freeze-drying, then infiltrated them with HT epoxy to form dense composites. The BNNT foam exhibited the highest neutron radiation shielding, with a mass absorption coefficient of 26.64 $cm^2\ g^{-1}$, outperforming the hybrid foam (18.18 $cm^2\ g^{-1}$) and the BNNP foam (11.12 $cm^2\ g^{-1}$). A similar trend was observed in the HT epoxy composites; incorporating these foams at least doubled the mass absorption coefficient compared to the neat polymer. In terms of thermal conductivity, the BNNT/BNNP foam-epoxy composite achieved the highest value of 0.34 W $m^{-1}\ K^{-1}$, a 2.13-fold increase over neat HT epoxy. The BNNT/BNNP foam-epoxy composites also improved by 1.88 and 1.75 times, respectively. Mechanical testing revealed that BNNP foams withstood the highest loads during nanoindentation (3.53 kN), followed by BNNT/BNNP foams (1.93 kN) and BNNT foams (1.56 kN). All BN foam-epoxy composites exhibited enhanced damping properties, with tan δ increasing by at least 30 % compared to neat HT epoxy. These findings elucidate the impact of BN nanomaterial morphology on the multifunctional performance of HT epoxy composites, offering insights for developing high-performance, tailorable materials for demanding environments.

1. Introduction

The demand for lightweight, multifunctional polymer composites has driven extensive research into advanced composites, particularly those reinforced with nanomaterials. These composites must have multifunctional properties, such as effectively shielding neutron radiation, conducting thermal energy, and dissipating mechanical energy. Neutron radiation shielding is a crucial requirement for materials used in space exploration, as it reduces health risks for astronauts, prevents electronic operation failures, and mitigates material degradation during extended missions [1]. Galactic Cosmic Rays (GCR) and Solar Particle Events (SPE) generate secondary radiation, including neutrons, significantly contributing to the radiation dose absorbed by crew members on deep space missions [2]. Neutron radiation can adversely affect electronics by inducing single-event effects, leading to data corruption, operational malfunctions, and even permanent damage to electronic components [3,4].

Furthermore, neutron radiation can cause atomic displacements and

* Corresponding author.
E-mail address: agarwala@fiu.edu (A. Agarwal).

https://doi.org/10.1016/j.compscitech.2024.110995
Received 25 September 2024; Received in revised form 27 October 2024; Accepted 3 December 2024
Available online 4 December 2024

create defects within material structures, resulting in embrittlement, swelling, and changes in mechanical properties [5]. This displacement damage ultimately compromises the strength and integrity of the material [6]. An additional key requirement for these materials is their effective thermal management, which is essential in space environments where thermal cycling can affect the functionality and durability of materials and equipment [7]. High thermal conductivity helps dissipate heat efficiently, thereby preventing overheating and ensuring stable operation [8]. Additionally, the ability to dissipate mechanical energy is crucial for components subjected to dynamic loads and vibrations during launch, space travel, landing, and on-site dynamic operations [9]. This capability reduces the risk of mechanical fatigue and failure, enhancing the durability and reliability of spacecraft structures [10].

Boron nitride (BN) has garnered significant attention among the various nanomaterials due to its exceptional mechanical, thermal, chemical, and neutron radiation shielding properties. Boron nitride nanomaterials can be synthesized in multiple morphologies, including zero-dimensional (0D) quantum dots, one-dimensional (1D) nanotubes (BNNT), and two-dimensional (2D) nanoplatelets (BNNP), each offering unique advantages for composite reinforcement.

BNNTs are 1D tubular nanostructures of boron and nitrogen atoms arranged in a hexagonal lattice [11]. These nanotubes have a high aspect ratio with diameters typically in the nanometer range and lengths extending to several micrometers. BNNTs are known for their high elastic modulus, reaching up to 1.3 TPa, providing exceptional mechanical strength [12]. They also exhibit remarkable thermal properties, maintaining thermal stability at temperatures above 800°C in air and a thermal conductivity of 200 $W\,m^{-1}\,K^{-1}$ [13]. BN-based nanomaterials offer excellent neutron radiation shielding due to the high thermal neutron capture cross-section of ^{10}B, which can reach up to 3835 *barns* [1]. In addition, due to their high aspect ratio, BNNTs can efficiently absorb and dissipate mechanical energy through their deformable tubular structure [14].

BNNPs, on the other hand, are 2D sheet-like structures composed of boron and nitrogen atoms arranged in a hexagonal lattice [15]. BNNPs present a similar structure to graphene but with alternating boron and nitrogen atoms instead of carbon. BNNPs offer similar thermal stability, remaining stable at temperatures up to 850°C in air and thermal conductivity of up to 600 $W\,m^{-1}\,K^{-1}$ along its basal plane [16]. The mechanical properties of BNNPs provide significant reinforcement potential with an elastic modulus of around 0.7 TPa. The 2D layered structure of BNNPs allows for interlayer sliding and energy dissipation. The high aspect ratio and large surface area of BNNPs enhance mechanical damping and prevent localized deformation, maintaining structural integrity under dynamic loads [17]. These properties make both 1D BNNTs and 2D BNNPs ideal candidates for enhancing the neutron radiation shielding, thermal, and damping performance of polymer composites.

The fabrication of polymer nanocomposites presents substantial challenges, primarily due to the tendency of nanomaterials to agglomerate owing to $\pi - \pi$ stacking forces and van der Waals interactions [18]. This agglomeration often results in an uneven distribution of nanomaterials within the polymer matrix, leading to compromised material properties [19]. Freeze-drying offers a solution to polymer nanocomposite fabrication by forming interconnected nanomaterial networks that serve as the backbone or foundational framework for polymer matrices [20]. Freeze-drying not only effectively prevents nanomaterial agglomeration but also allows for the controlled design of foam microstructures, enabling the tailoring of material properties [16]. Through precise control of thermodynamic parameters during freeze-drying, the microstructure of these foams can be designed [21]. Factors such as freeze-drying solid loading, nanomaterial size, foam density, mold material, and geometry are crucial in shaping the final foam microstructure. For instance, higher solid loading results in denser foams, while nanomaterial size and mold geometry variations influence pore orientation and distribution.

These ultralightweight and highly porous foams can be infiltrated with liquid polymers like high-temperature (HT) epoxy to produce dense nanocomposites. Vacuum-assisted infiltration ensures thorough impregnation of liquid polymer matrices throughout the foam, yielding a uniformly reinforced composite material. This approach enhances the interaction between the polymer matrix and the 3D nanomaterial network by ensuring complete penetration of the epoxy into the intricate foam microstructure. As a result, the composite exhibits improved radiation shielding, thermal, and damping properties.

In this study, ultralightweight lamellar BN foams, including BNNT, BNNP, and hybrid BNNT/BNNP foams and their corresponding high-temperature (HT) epoxy composites were fabricated *via* freeze-drying and vacuum-assisted infiltration. These foams and composites were characterized in terms of their radiation, thermal, and mechanical properties. This study aims to elucidate the radiation shielding, thermal conduction, and damping mechanisms of BN foams and polymer composites. The freeze-drying fabrication process and its underlying thermodynamic parameters were correlated with the BN nanomaterial morphology, whether 1D nanotubes or 2D nanoplatelets.

The microstructure of the BN foams and BN foam-HT epoxy composites was investigated with a focus on the effect of 1D and 2D BN nanomaterial morphologies through Scanning Electron Microscopy (SEM) and microcomputed tomography (μ-CT). The neutron radiation shielding properties of the BN foams and composites were characterized *via* indium foil activation tests. The thermal conductivity of the BN foams and their composites was measured using flash diffusivity.

In-situ nanoindentation was used to study the mechanical behavior of the foams, providing real-time visualization of deformation along with the load-displacement relationship. The mechanical behavior of the BN foam-HT epoxy composites under dynamic loading was studied using sinusoidal nanoindentation to obtain a foundational understanding of the strengthening mechanisms of 1D BNNT and 2D BNNP. In summary, this study aims to establish an analytical framework establishing the connection between the fabrication, microstructure, and properties of 1D and 2D BN nanomaterial-HT epoxy composites for innovations in aerospace, automotive, sports equipment, and other industries.

2. Methods

2.1. BN-Nanomaterial characterization

Hexagonal boron nitride (hBN) nanoplatelets, referred to as boron nitride nanoplatelets (BNNP), were purchased from pH Matter Inc. (Columbus, Ohio, USA). These BNNP particles exhibit a flake-like morphology with sizes ranging from 100 nm to 3 μm in their basal direction and thicknesses between 40 to 65 nm. Purified boron nitride nanotubes (BNNTs) synthesized through a pressurized vapor condensation method were obtained from BNNT, LLC (Newport News, Virginia). These BNNTs typically have diameters ranging from about 5 to 10 nm and can be up to 100 μm long. The BNNTs are highly entangled and agglomerated, forming bundled structures.

The microstructure of these particles was examined using a Scanning Electron Microscope (SEM JEOL JSM-F100, JEOL Ltd., Tokyo, Japan). Prior to analysis, the particles were dispersed using tip sonication (Vibra-Cell VCX750, Sonics & Materials, Inc., Newtown, CT, USA) with a 19 mm tip diameter at 40% amplitude for 30 min. Before imaging, the nanoparticles were coated with gold particles using vacuum sputtering.

2.2. Fabrication of BN foams

Three types of highly dispersed, lightweight BN nanomaterial-based foams were synthesized through a freeze-drying method. The types include foams composed of boron nitride nanotubes (BNNT foam), boron nitride nanoplatelets (BNNP foam), and a hybrid combination of both (BNNT/BNNP foam). Deionized water was used as the freezing

agent. At the same time, styrene-butadiene rubber (SBR, MTI Corporation, Richmond, CA, USA) served as the binding agent to maintain the structural integrity of the boron nitride nanoparticle scaffold post-sublimation. Sodium carboxymethyl cellulose (CMC-Na, Mw ~ 700,000, Millipore Sigma, Burlington, MA, USA) was utilized as the dispersing agent. The composition of the freeze-drying slurry was established at 93 wt.% deionized water, 2 wt.% SBR, and 1 wt.% CMC-Na. The BNNT/BNNP foams were prepared by adding 4 wt.% of BNNTs and BNNPs, respectively, into the slurry. The hybrid BNNT/BNNP foam was prepared by adding 3.5 wt.% of BNNPs and 0.5 wt.% of BNNTs. Before preparing the slurry for BNNT and hybrid BNNT/BNNP foams, the BNNTs were dispersed in deionized water using tip sonication (Vibra-Cell VCX750, Sonics & Materials, Inc., Newtown, CT, USA). The sonication was performed with a 750 – watt sonicator at 40% amplitude, operating in cycles of 60 sec on and 30 sec off for a total duration of 30 min.

The slurry preparation process began with the vortex mixing of CMC-Na and SBR in deionized water at ambient temperature for 30 min. Then, BN nanoparticles were added and vortex-mixed for an additional 1 h. The solution was then bath-sonicated (Bransonic Ultrasonics Corporation, 3510R-DTH, Danbury, CT, USA) at 42 kHz for 30 min to ensure a well-dispersed slurry of BN nanoparticles. This slurry was subsequently poured into aluminum molds. The slurry-filled molds were frozen for 4 h at −56°C under ambient pressure, followed by a sublimation process lasting 24 h at the same temperature at a lower pressure of 1 Pa, conducted in a freeze-dryer (Pro-Freeze Dryer PLT300, ProLab Inc., Fort Worth, TX, USA). Ultra-lightweight, free-standing porous networks of BN nanomaterials or BN foams were obtained.

The density of the BN foams was measured *via* geometric density. The density of the BNNT foams was 0.040 ± 0.005 g cm^{-3}, while that of the BNNT/BNNP foams was 0.050 ± 0.005 g cm^{-3}, and that of the BNNP foams was 0.050 ± 0.003 g cm^{-3}.

The porosity $\left(f_p\right)$ of the BN foams was determined using the geometric density of the foams $\left(\rho_{foam}\right)$ and the composite bulk material density $\left(\rho_{composite}\right)$. The BN composite bulk density was estimated using the rule of mixtures, considering the following component densities: $\rho_{BNNP} = 2.1\ g\ cm^{-3}$, $\rho_{BNNT} = 2.2\ g\ cm^{-3}$, $\rho_{SBR} = 0.95\ g\ cm^{-3}$, and $\rho_{CMC-Na} = 1.6\ g\ cm^{-3}$. The BN foam porosity was then calculated using the relationship in equation (1).

$$f_p = 1 - \frac{\rho_{foam}}{\rho_{composite}} \tag{1}$$

The porosity of the BNNT foams was $97.50 \pm 0.05\%$, while that of the BNNT/BNNP foams was $97.07 \pm 0.02\%$, and that of the BNNP foams was $97.04 \pm 0.01\%$.

2.3. Fabrication of BN Foam-HT epoxy composites

The BN foam-HT epoxy composites were fabricated using the vacuum-assisted infiltration technique. A two-component high-temperature (HT) epoxy (EP114, Master Bond, New Jersey, USA) was infiltrated into the free-standing BN foams. The two-component HT epoxy (containing epoxy resin and curing agent) was heated to 80°C for 1 h to reduce their viscosity and facilitate infiltration. The epoxy resin-to-hardener ratio of 50:40 was achieved by mixing with a vortex to obtain a homogeneous solution. The HT epoxy solution was poured over the BN foams to initiate infiltration and placed under vacuum at 1 Pa for 90 min. Once the foam was fully infiltrated, the HT epoxy was cured by heating the mixture to 80°C for 30 min for moisture removal. Then, the solution was heated to 125°C at 1°C/min and maintained at this temperature for an isotherm period of 3 h. After this, heating continued at 1°C/min until the temperature reached 150°C, and this temperature was held for an isotherm period of 6 h. Then, the HT epoxy was heated at the same rate of 1°C/min until the temperature reached 200°C and was maintained for another isotherm period of 4 h. Finally, the HT epoxy slowly returned to room temperature.

2.4. Microstructure characterization

Field emission scanning electron microscopy (FE-SEM JEOL JSM-F100, JEOL Ltd., Tokyo, Japan) and energy dispersive X-ray spectroscopy (EDS) were used to examine the microstructure of the BN foams and their corresponding HT epoxy composites. Before imaging and EDS analysis, the foam samples were coated with gold particles using vacuum sputtering. An electron-accelerating voltage of 3 kV was employed for imaging, and 10 kV was used for EDS to determine the elemental composition of the foams.

Micro-computed tomography (μ-CT) scans (SkyScan 1272 CMOS) were used to obtain a 3D reconstruction of the BN foams. Scans were performed using a voxel size of 4 μm, with a source voltage of 50 kV and a source current of 200 μA. The scans incorporated an exposure time of 750 ms and a rotation step of 0.1°. ImageJ, an image processing software, was used to analyze the μ-CT scans, as shown in Supplementary Fig. 1. The μ-CT scan videos of the BNNT foam, BNNT/BNNP foam, and BNNP foams can be observed in **Supplementary Videos 1, 2, and 3,** respectively**.**

2.5. Neutron radiation shielding characterization

The radiation shielding tests were conducted at NASA Langley Research Center using the LaRC Radiation Test Facility. The neutron source was a 1 Ci Americium/Beryllium (Am/Be) radioactive source, producing fast neutrons (4.5 MeV). The detection foil was a 1.25″ Indium foil (0.5 mm,19 barns). To moderate the neutron energy to mostly thermal neutrons (< 0.5 eV), a polyethylene (PE) block was placed between the source and the sample. The exposed equivalent dose rate was 320 mrem/hr, measured with a Ludlum Portable Survey Neutron meter (Model 2363) and a Prescila proton recoil scintillator probe (Model 42-41L) with a detection range of 0.1 mrem/hr to 1 rem/hr. The foams were secured in a plastic sample box to maintain the BN foam integrity, ensuring that the sample holders did not affect the radiation shielding measurements.

2.6. Thermal conductivity characterization

The thermal conductivity of the BN foams and their HT epoxy composites was measured using a laser flash technique (NETZSH LFA 467 HT HyperFlash, Selb, Germany). The foams and composites were cut into 10 mm-length squares with 4.0 ± 0.1 mm thickness. The test was conducted at temperatures between 25 and 100 °C, with a 15 °C/step. The foams and composites were oriented so that the BN foam lamellar walls were parallel to the heat transfer direction.

2.7. Nanomechanical behavior of BN foam

2.7.1. In-situ nanoindentation

In-situ quasi-static nanoindentation tests were conducted to assess the mechanical behavior of BN foams under localized stress. The tests were conducted using a Picoindenter (Hysitron PI 87, Minnesota) mounted on the stage of a field-emission scanning electron microscope (FE-SEM JEOL JSM-F100, JEOL Ltd., Tokyo, Japan). This setup allowed for real-time SEM imaging of strain development within the microstructure of the foam relative to the applied indentation force. The foams were strategically aligned so that their lamellar walls were either parallel or perpendicular to the direction of the nanoindentation load. A titanium cylindrical flat punch tip with a 500 μm diameter was used to apply precisely localized loads, selected for its low-stress concentration, thereby mimicking compression in the targeted areas. Displacement-controlled *quasi-static* nanoindentation was applied with a maximum displacement of 150 μm and a loading/unloading rate of 10 μm/s. This

indentation depth was selected to sufficiently deform the foam to reveal the hierarchical organization of its interconnected walls and bridges.

2.8. Damping behavior of the BN Foam-HT epoxy composites

Dynamic tests were conducted to assess the damping behavior of the BN foam-HT epoxy composites using a Hit 300 nanoindenter (Anton Paar, Graz, Austria). A nanoindentation continuous stiffness measurement sinusoidal mode was selected to capture the time-dependent properties of the polymer composites. The tests employed a Berkovich tip geometry and focused on measuring the tan delta values (loss and storage modulus). A maximum load of 80 mN with a 10 s holding section was applied. A strain rate of 0.5 1/s with an amplitude of 25 mN, and a frequency of 10 Hz was applied—ten indents with an indentation spacing of 0.1 mm. The data was analyzed using the Sinus Mean Model. For accurate testing, samples were polished to expose the 2D material layers and ensured to be flat for nanoindentation.

3. Results and discussion

3.1. Design of boron nitride foam microstructure via freeze-drying

The properties of BN-based composites with varying BN morphologies—specifically 1D BNNT and 2D BNNP—were explored by fabricating three types of highly dispersed, lightweight BN foams using freeze-drying. These foams include BNNTs, BNNPs, and a hybrid combination of BNNT/BNNP. The BN foams are 3D free-standing networks of BN nanomaterials that are ultralightweight and highly porous, exhibiting a lamellar microstructure as shown in the SEM micrographs of Fig. 1. The formation of the lamellar microstructures in BN foams can be attributed to the characteristics of the BN nanomaterials and the freeze-drying process. Previous studies have shown that low-density 2D materials, such as BNNP, tend to form lamellar structures due to the resistive and repulsive forces they experience during freeze-drying. This contrasts with higher-density materials like WS_2, which form reticulated structures[21].

The density of the BNNT foams was 0.040 ± 0.005 g cm^{-3} with a porosity of $97.50 \pm 0.05\%$, while the density of the BNNT/BNNP foams was 0.050 ± 0.005 g cm^{-3} with a porosity of $97.07 \pm 0.02\%$, and the density of the BNNP foams was 0.050 ± 0.003 g cm^{-3} with a porosity of $97.04 \pm 0.01\%$.

The microstructures of the BNNT, BNNT/BNNP, and BNNP foams can be observed in Fig. 1a, b, and 1c, respectively. Each figure shows a high-magnification micrograph of each foam, highlighting the individual BN nanomaterials that compose a single foam wall. Fig. 1a shows individual 1D BNNT tubular structures that form a wall. In turn, Fig. 1c reveals single sheet-like 2D BNNP structures forming a foam wall. Fig. 1b displays a mixture of BNNTs and BNNPs, indicating a hybrid morphology.

While all the foams exhibited a lamellar microstructure, variations in wall thickness and distance between walls (wall gap) were observed. Fig. 1d quantifies the wall thickness, showing that the BNNT foam had the thinnest walls at 0.99 ± 0.15 μm, the BNNP foam had the thickest walls at 4.32 ± 0.58 μm, and the BNNT/BNNP foam had an intermediate wall thickness of 3.04 ± 0.93 μm. As a result, the wall gap was lowest for the BNNT foam at 27.46 ± 3.68 μm, followed by the BNNT/BNNP foam at 65.73 ± 8.64 μm, and the BNNP foams at 100.92 ± 19.79 μm, as shown in Fig. 1e.

These differences can be attributed to the behavior of different BN nanomaterial morphologies during freeze-drying. As shown in Fig. 1f, the BN particle shape or morphology significantly influences the resulting foam microstructure. During freezing, the nanoparticles surrounded by the freezing agent experience gravitational and frictional forces. The gravitational forces (F_g) acting on the BN particles during the freeze-drying process, which is defined by the Archimedes principle and heavily depends on the nanoparticle volume. The relationship in equation (2) represents the gravitational forces.

$$F_g = (m - \rho_l V)g \tag{2}$$

Here, m is the nanoparticle mass, ρ_l is the freezing agent density, V is the nanoparticle volume, and g is the force of gravity. On the other hand, the frictional forces (F_f) acting on the BN particles during freeze-drying are defined by Stoke's law and greatly depend on the nanoparticle surface area. The relationship in equation (3) represents these frictional forces.

$$F_f = \int_0^A \tau dA = \int_0^A \mu \frac{du}{dy} dA \tag{3}$$

Here, A is the nanoparticle surface area, τ is the shear stress, μ is the liquid viscosity, and $\frac{du}{dy}$ is the velocity gradient. BNNTs have a high surface area-to-volume ratio and, thus, experience higher frictional forces. These frictional forces easily overcome gravitational forces, forming thinner foam walls and smaller wall distances. In contrast, BNNPs, with their lower surface area-to-volume ratio, result in thicker foam walls due to lower frictional forces. Consequently, the hybrid BNNT/BNNP foam exhibits intermediate wall thickness and gap due to the combination of both nanostructures.

The freeze-drying process allows control over the BN foam microstructure, facilitating the design of composites with tailored properties. Incorporating 1D BNNTs and 2D BNNPs enhances the versatility of these materials, enabling the creation of composites with optimized performance.

The BN foams were subsequently infiltrated with liquid HT epoxy by pouring the uncured polymer solution, consisting of epoxy resin and curing agent, on top of the foam under vacuum, as shown in Fig. 2a. Under vacuum conditions, the liquid polymer is forced to infiltrate the porous network within the BN foam walls, as demonstrated in Fig. 2b. Once the HT epoxy fully infiltrated the BN foams, the polymer was cured to obtain the BN-HT epoxy composites, as illustrated in Fig. 2c. A micrograph of the fully HT epoxy-infiltrated BNNT foam can be observed in Fig. 2d. While the epoxy fully infiltrated the BNNT foam structure, it can be observed that the BNNT foam structure was retained as the foam walls were visible.

Similarly, the hybrid BNNT/BNNP foam-HT epoxy composite can be observed in Fig. 2e. Finally, the BNNP foam-HT epoxy composite can be observed in Fig. 2f. Higher magnification micrographs, observed in Fig. 2g, h, and 2i, show the individual BN nanoparticles that compose the BNNT, BNNT/BNNP, and BNNP foam walls, respectively. The density of HT epoxy was 1.29 ± 0.01 g cm^{-3}. The density of the BNNT foam-HT epoxy composite was 1.28 ± 0.06 g cm^{-3}, while the density of BNNT/BNNP foam-HT epoxy was 1.30 ± 0.01 g cm^{-3}, and the density of the BNNP foam-HT epoxy composite was 1.27 ± 0.06 g cm^{-3}.

3.2. Effect of BN nanomaterial 1D vs 2D morphology on the neutron radiation shielding behavior of HT epoxy composites

In space, the main sources of radiation are GCR and SPE, which consist predominantly of high-energy protons and other particles. When these particles interact with matter, such as the lunar surface, they produce secondary radiation, which includes neutrons, as illustrated in Fig. 3a. Neutrons are a particular concern because they are uncharged, making them highly penetrating and challenging to shield against. This section explores the effect of different BN morphologies on the neutron radiation shielding performance of their HT epoxy composites, as shown in Fig. 3b.

The neutron radiation shielding performance of the composites was tested *via* indium foil activation tests. As shown in Fig. 1, the BN foams have a lamellar microstructure that leads to anisotropic properties. The samples were oriented such that their walls were perpendicular to the

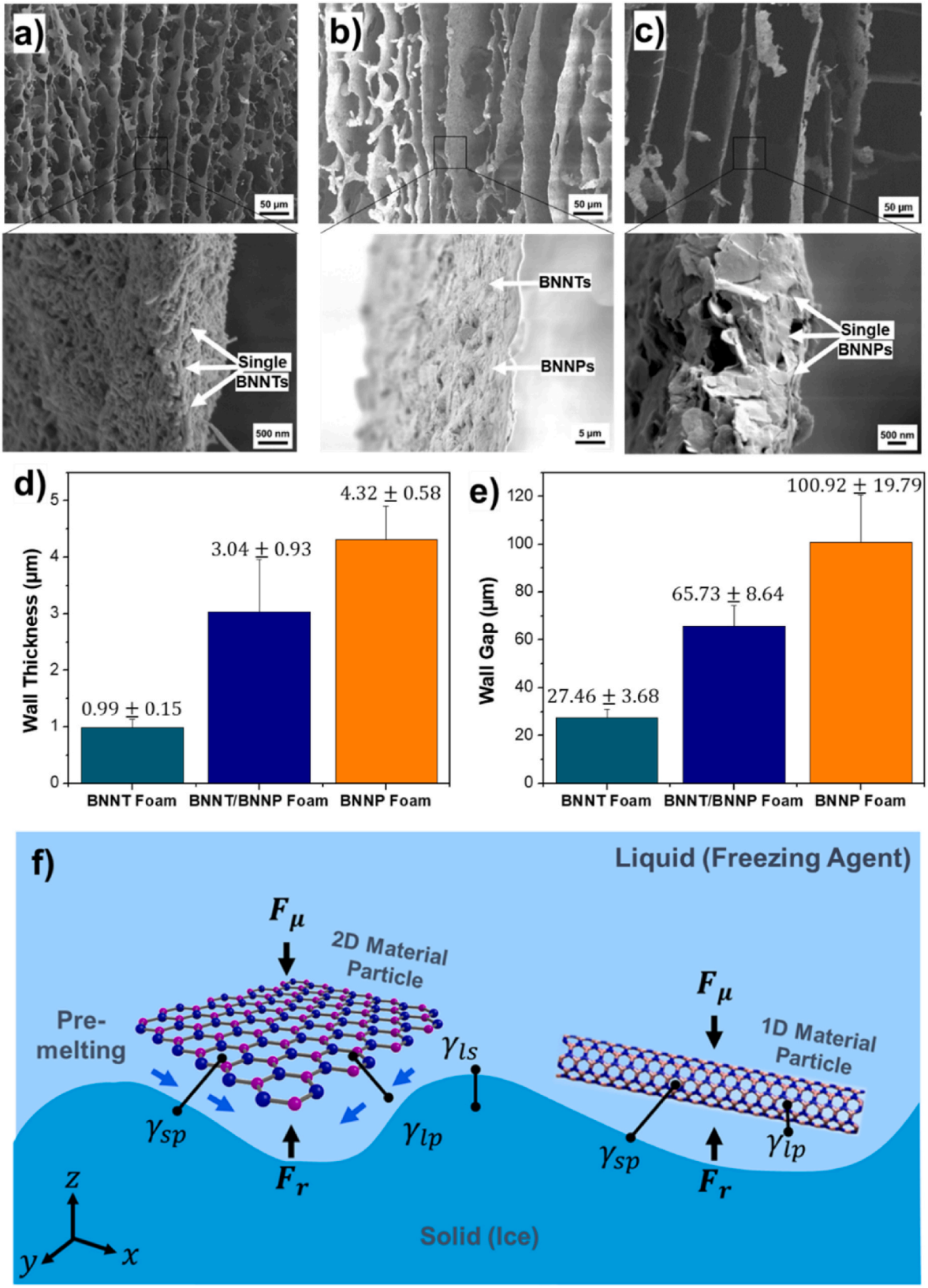

Fig. 1. Correlation between 1D BNNT and 2D BNNP foam freeze-drying processing and microstructure: a) BNNT foam, b) BNNT/BNNP foam, c) BNNP foam, d) wall thickness as a function of 1D vs 2D BN nanomaterial, e) wall gap as a function of 1D vs 2D nanomaterial, f) BN nanomaterial morphology-dependent freeze-drying forces.

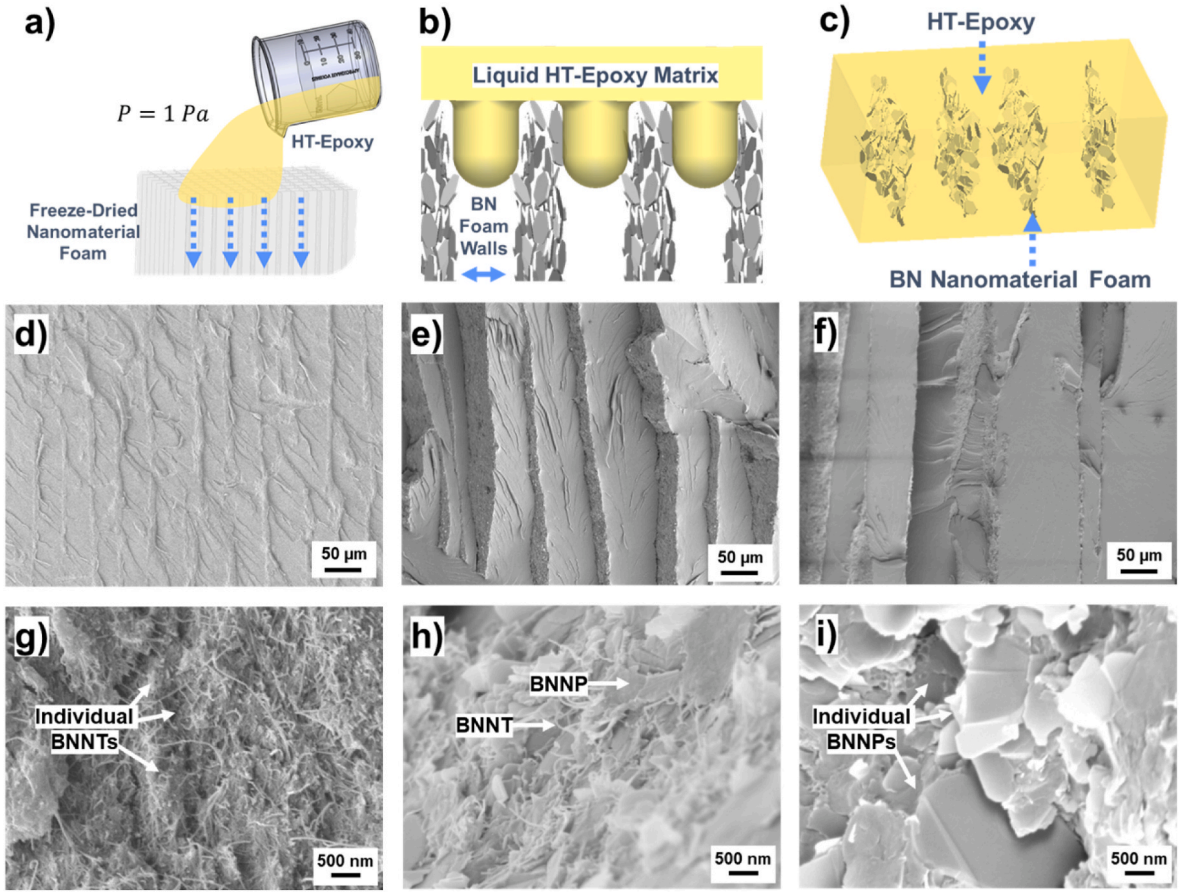

Fig. 2. a) Vacuum-assisted infiltration of HT epoxy into BN foams, b) interaction between liquid HT epoxy and BN foam walls, c) resulting BN-HT epoxy composite, fracture surface microstructure of HT epoxy composites reinforced with d) BNNT foam, e) BNNT/BNNP foam, and f) BNNP foam, and high magnification micrograph of BN foam walls composed of individual g) BNNTs, h) BNNTs/BNNPs, and i) BNNPs.

direction of the neutron source to evaluate the neutron radiation shielding capabilities of foams.

In this study, we focused our neutron shielding analysis on the perpendicular orientation of the BN foam composites, where this BN wall orientation maximizes the interaction with the neutron source. This orientation is particularly relevant for practical applications, as it leverages the lamellar microstructures of the BN foams to enhance neutron attenuation. Previous research has demonstrated the anisotropic properties of BN foams, and the current study emphasizes the performance differences between BN nanotubes and nanoplatelets[16]. Additionally, we highlight that the lamellar structures observed *via* SEM are consistent throughout the bulk of the material, as supported by the μ-CT results.

The mass absorption coefficient of the BN foams can be observed in Fig. 3c, which is used to quantify the neutron radiation shielding effectiveness of the materials. The mass absorption coefficient μ_m of materials is defined by the Beer-Lambert law represented in equation (4).

$$\mu_m = \frac{\mu}{\rho} = \frac{1}{\rho X} ln\left(\frac{I_0}{I}\right) \quad (4)$$

Here, μ is the linear absorption coefficient, ρ is the shielding material density, X is the shielding material thickness, I_0 is the number of transmitted neutron fluxes without the shielding material, and I is the number of transmitted neutron fluxes with the shielding material.

As can be observed in Fig. 3c, the 1D BNNT foam presented the highest mass absorption coefficient at 26.64 $cm^2\ g^{-1}$, the 1D BNNT/2D BNNP foam had an intermediate value of 18.18 $cm^2\ g^{-1}$ and the 2D BNNP foam had the lowest value of 11.12 $cm^2\ g^{-1}$.

These differences in mass absorption coefficients may be attributed to variations at both the microscale and nanoscale levels. In the microscale, this variation can be attributed to differences in foam morphology, specifically the surface area among the three foams, as shown in Fig. 1. The BNNT foams had a higher surface area due to their higher number of walls, with a wall thickness of 0.99 ± 0.15 μm and a lower wall gap of 27.46 ± 3.68 μm. In contrast, the BNNP foam had thicker walls of 4.32 ± 0.58 μm and a wall gap of 100.92 ± 19.70 μm, while the BNNT/BNNP foam had an intermediate wall thickness of 3.04 ± 0.93 μm and a wall gap of 65.73 ± 8.64 μm. The higher surface area of BNNT foams exposes more 10B atoms, which are available to capture neutrons *via* the neutron capture mechanism. In contrast, the lower number of walls in the BNNP foam structure leads to lower exposure of 10B atoms, reducing the surface available for neutron capture. Consequently, the hybrid BNNT/BNNP foam presents an intermediate behavior due to its intermediate wall thickness and wall gap.

These variations in mass absorption coefficients could also be attributed to nanoscale differences, specifically the surface area-to-volume ratio of the BN nanomaterial particles. It is well-known that BNNTs have a higher surface area-to-volume ratio than BNNPs. For instance, BNNTs typically exhibit specific surface areas ranging from 200 to 4 00 m^2g^{-1}, while BNNPs generally have specific surface areas between 100 to 200 m^2g^{-1} [12,22–24]. The increased surface area-to-volume ratio of BNNTs means that more boron atoms are available on the foam wall surface for neutron interactions, thereby improving the overall neutron shielding efficiency. In contrast, the lower surface area-to-volume ratio of BNNPs results in fewer boron atoms being exposed on the surface, which may reduce their

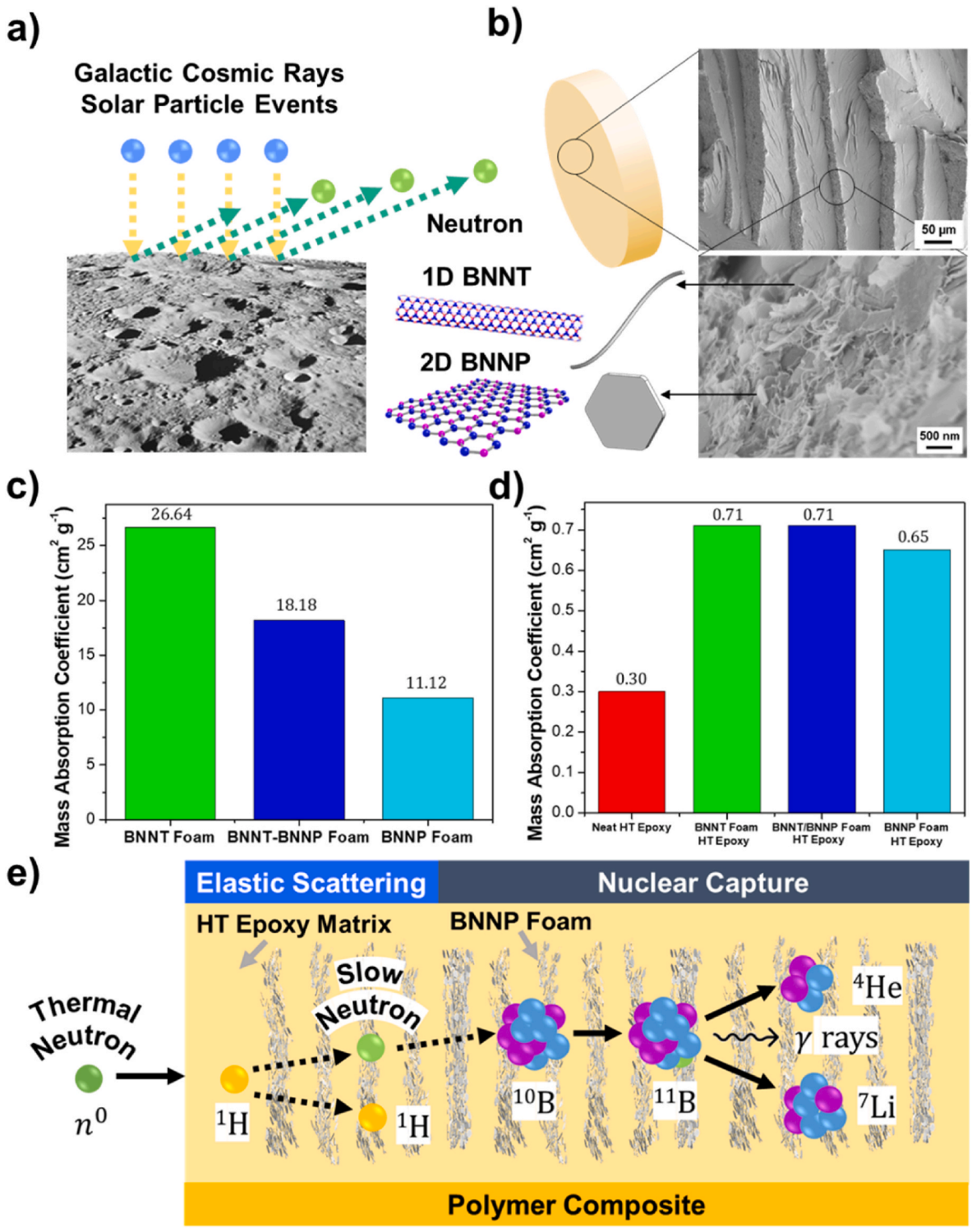

Fig. 3. Neutron radiation shielding performance of BN foams and HT epoxy composites: a) interaction of GCR and SPE with matter producing secondary neutrons, b) SEM images of BN foams with BNNTs, BNNPs, and a combination, mass absorption coefficients of c) BN foams, and d) BN foam-HT epoxy composites, and e) neutron shielding mechanisms: elastic scattering and nuclear capture.

effectiveness in neutron capture. It is important to emphasize that further investigation is needed to validate these surface area mechanisms at both the microscale and nanoscale levels within the foams.

The neutron capture mechanism of BN nanomaterials relies on the high thermal neutron capture cross-section of 10B, which is 3835 barns. This neutron capture cross-section is the largest among the low atomic number elements [11]. When a 10B atom captures a thermal neutron, it undergoes the reaction in equation (5).

$$10B + n \rightarrow 7Li + \alpha + \gamma \quad (5)$$

The nuclear capture of 10B reaction results in the release of 7Li, an alpha particle, and gamma radiation. Otherwise, the thermal neutrons are likely to be scattered by 1H, which is present in the binding (SBR) and dispersing (CMC-Na) agents, until they either collide with a 10B

atom or are transmitted through the material thickness.

The mass absorption coefficient of neat HT epoxy and the corresponding BN foams-HT epoxy composites can be observed in Fig. 3d. The mass absorption coefficient of neat HT epoxy is 0.30 $cm^2 g^{-1}$. The BNNT foam-HT epoxy and BNNT/BNNP foam-HT epoxy both exhibited a mass absorption coefficient of 0.71 $cm^2 g^{-1}$, while the BNNP foam-HT epoxy was lower at 0.65 $cm^2 g^{-1}$. Notably, the inclusion of any foam significantly increased the mass absorption coefficient of the HT epoxy, at least doubling it. Specifically, the BNNT foam-HT epoxy and BNNT/BNNP foam-HT epoxy composites showed 2.37 times better neutron radiation shielding compared to the neat HT epoxy, while the BNNP foam-HT epoxy composite exhibited a 2.17 times improvement. It is worth highlighting that the difference in mass absorption coefficient values between the foams and their composites is due to their difference in density. The density of the materials normalizes the mass absorption coefficient, and thus, the polymer composites, which are much denser than the foams themselves, have higher values.

The BN foam-HT epoxy neutron shielding mechanisms involve elastic scattering and nuclear capture. Isotopes with a similar mass to neutrons, such as 1H, induce significant energy loss during elastic scattering. HT epoxy facilitates effective neutron scattering due to its abundant 1H content. Subsequently, slow neutrons are captured by 10B, which has an exceptionally large thermal neutron absorption cross-section of 3835 barns. Fig. 3e depicts the neutron radiation shielding mechanism present in the BN foam-HT epoxy composites, highlighting the roles of elastic scattering and nuclear capture in enhancing the shielding performance of these advanced materials. The differences observed between the BNNT foam-HT epoxy, BNNT/BNNP foam-HT epoxy, and BNNP foam-HT epoxy can be linked to the foams' neutron radiation shielding behavior. The observed variation in mass absorption coefficient values can be attributed to the BNNT particles having a higher surface area-to-volume ratio compared to BNNPs.

3.3. *Effect of BN nanomaterial 1D vs 2D morphology on the thermal behavior of HT epoxy composites*

This section examines the impact of different BN morphologies (1D BNNTs and 2D BNNPs) on the thermal conductivity of BN foams and their HT epoxy composites. Thermal conductivity tests were conducted using flash diffusivity, as illustrated in Fig. 4a. As shown in Fig. 1, the BN foams exhibit a lamellar microstructure, resulting in anisotropic properties. To compare the thermal properties of the 1D BNNT, 1D BNNT/2D BNNP, and 2D BNNP foams, the foams were oriented with their walls parallel to the heat transfer direction. The thermal conductivity of the BN foam composites was primarily evaluated in the parallel configuration, where heat transfer aligns with the BN walls, to highlight the differences between BN nanotubes and nanoplatelets. Previous studies have demonstrated the anisotropic thermal conductivity of BN foams, with significant variation between the parallel and perpendicular directions due to the lamellar structure[21]. In this study, we focus on the

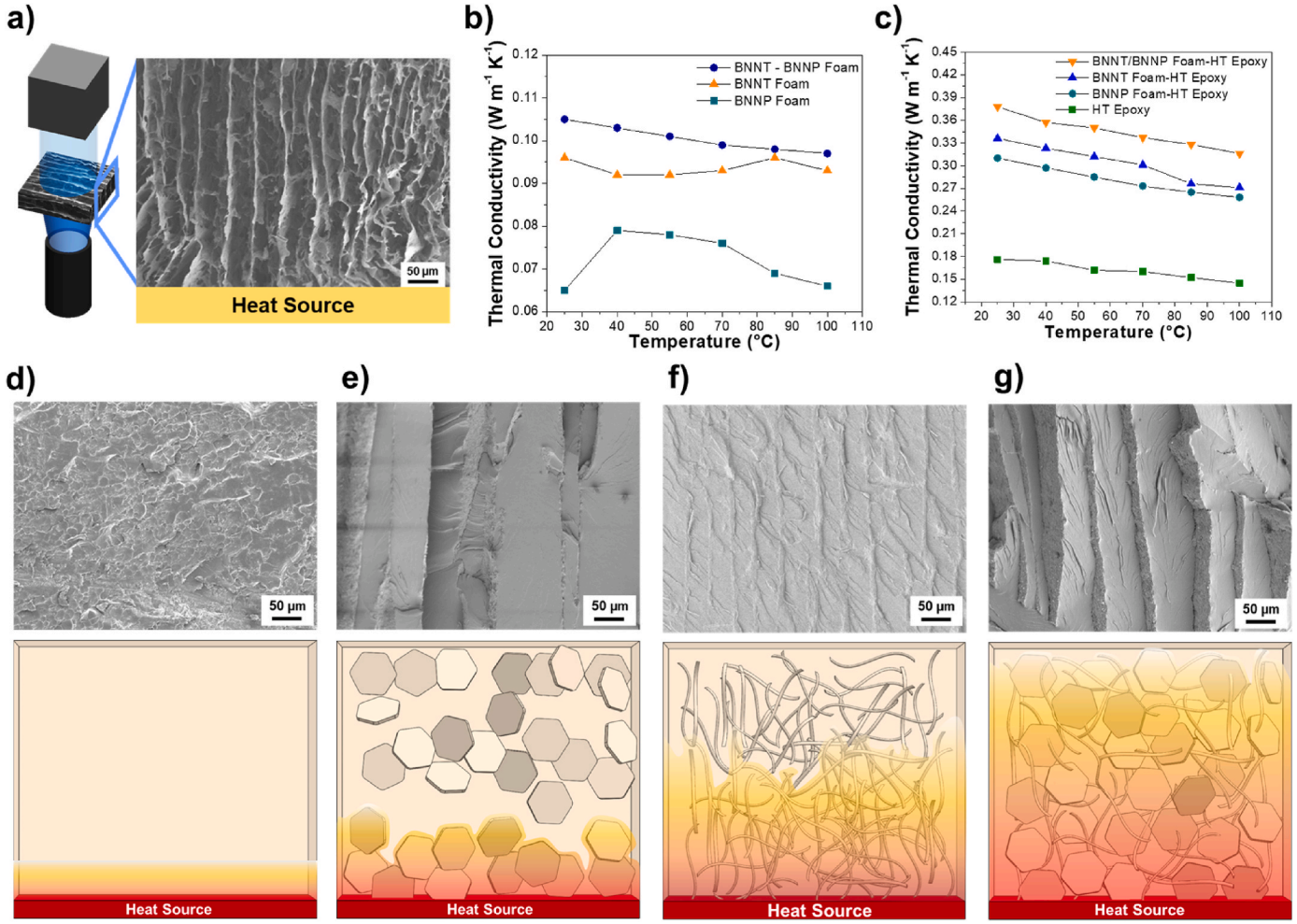

Fig. 4. Thermal conductivity of BN foam-HT epoxy composites: a) flash diffusivity setup for thermal conductivity testing, the thermal conductivity of b) BN foams, and c) BN foams-HT epoxy composites. Microstructure of d) neat HT epoxy, e) BNNP-HT epoxy, f) BNNT-HT epoxy, and g) BNNT/BNNP-HT epoxy.

parallel direction to assess the dominant heat transfer pathways.

Fig. 4b shows the thermal conductivity of the BN foams as a function of temperature. It is observed that the hybrid BNNT/BNNP foam presented the highest thermal conductivity of 0.10 ± 0.00 W $m^{-1}K^{-1}$ among all the foams. The BNNT foam had an intermediate conductivity of 0.09 ± 0.00 W $m^{-1}K^{-1}$, while the BNNP foam had the lowest, 0.07 ± 0.0 W $m^{-1}K^{-1}$.

The variations in thermal conductivity can be attributed to the differences in foam morphology, which determine the phonon transport pathways throughout the foams and composites. In neat HT epoxy, phonon scattering is the principal thermal transfer mechanism due to the lack of phonon transport pathways. The presence of BN nanomaterials introduces more efficient pathways for phonon transport within the material. However, different BN foam morphologies create unique transfer pathways with varying lengths, influencing the speed at which phonons can travel.

The lower thermal conductivity of BNNP foams can be attributed to the shorter 2D BNNP structure, which results in less interconnected pathways, slowing phonon movement. The intermediate thermal conductivity observed in BNNT foams might be due to the fact that 1D BNNTs provide longer, more continuous pathways, facilitating faster phonon transport. The highest thermal conductivity observed in hybrid BNNT/BNNP foams could be due to the synergistic effect created by the combination of both 1D and 2D nanostructures to create a well-interconnected scaffold that facilitates efficient phonon transport.

Fig. 4c shows the thermal conductivity of neat HT epoxy and the BN foams-HT epoxy composites. Neat HT epoxy presented a thermal conductivity of 0.16 ± 0.01 W m^{-1} K^{-1}. A similar trend is observed with the BN foams, where the hybrid BNNT/BNNP foam-HT epoxy exhibited the highest thermal conductivity of 0.34 ± 0.02 W m^{-1} K^{-1}, representing a 2.13 times increase compared to neat HT epoxy. The BNNT foam-HT epoxy had an intermediate thermal conductivity of 0.30 ± 0.03 W m^{-1} K^{-1}, which is 1.88 times higher than that of the neat HT epoxy, while the BNNP foam-HT epoxy had the lowest thermal conductivity of 0.28 ± 0.02 W m^{-1} K^{-1}, showing a 1.75 times improvement. Similarly, the thermal conductivity variations between the BN foam-HT epoxy composites can be correlated with the observed BN foam trend. Fig. 4d shows the microstructure of neat HT epoxy, while Fig. 4e, f, and 4g show the microstructures of BNNP-HT epoxy, BNNT-HT epoxy, and BNNT/BNNP-HT epoxy, respectively. These microstructures illustrate the differences in the internal scaffolding provided by the various BN morphologies. However, additional experiments are needed to confirm this theory and fully understand the mechanisms governing the thermal conductivity of these composites.

It is worth noting that the differences in thermal conductivity between the foams and the composites can be attributed to the presence of pores or air within the foams. Air has a low thermal conductivity of 0.025 W $m^{-1}K^{-1}$, approximately [25]. In contrast, the BN foam-HT epoxy composites are filled with HT epoxy, which has a significantly higher thermal conductivity of 0.16 ± 0.02 W $m^{-1}K^{-1}$.

These findings suggest that by optimizing the morphology of BN nanomaterials, we can develop advanced composites with tailored thermal properties specifically designed for various applications. By fine-tuning the balance between 1D and 2D BN structures, it becomes possible to create materials that offer control over thermal conductivity, making them ideal for use in environments that demand efficient heat dissipation. This control could be particularly beneficial in fields such as electronics, where managing heat is critical to maintaining performance and longevity, or in aerospace applications, where materials must endure extreme thermal conditions. The ability to engineer these properties through morphological adjustments opens up new possibilities for customizing materials to meet the unique thermal management needs of different industries.

3.4. Effect of BN nanomaterial 1D vs 2D morphology on the damping behavior of HT epoxy composites

The damping behavior of BN nanomaterial-reinforced HT epoxy composites is crucial for applications requiring vibration attenuation and mechanical energy dissipation. This section investigates the impact of different BN morphologies (1D BNNTs and 2D BNNPs) on the damping properties of BN foams and their HT epoxy composites. To fully understand the effect of adding BN foams into HT epoxy, the free-standing foams were characterized before infiltration. The mechanical characterization began with *in-situ* nanoindentation of the foams to assess their behavior.

Due to the lamellar microstructure of the foams, their mechanical behavior exhibits anisotropy. *In situ,* nanoindentation tests were performed by orienting the foams so that their walls were either parallel or perpendicular to the load direction to assess their anisotropy. Fig. 5 shows the mechanical characterization of the BN foams *via in-situ* nanoindentation. The maximum load during nanoindentation can be observed in Fig. 5a of the perpendicular foam wall orientations. The BNNP foams withstand the highest load at 3.53 kN, followed by BNNT/BNNP foams at 1.93 kN, and BNNT foams at 1.56 kN. The load-displacement curves in Fig. 5b further describe the mechanical response of the foams. The BNNP foam demonstrates the highest stiffness, followed by the BNNT/BNNP and BNNT foams. The microstructure of the BNNT, BNNT/BNNP, and BNNP foams under indentation in the perpendicular orientation can be observed in Fig. 5c to e.

Subsequently, the foams were characterized in a parallel orientation, with their walls aligned parallel to the nanoindentation load direction. Fig. 5f and g presents the maximum load and load-displacement curves for the composites, respectively. A similar trend was observed, where the BNNP foam-HT epoxy composite achieved the highest load of 6.09 kN, followed by the BNNT/BNNP foam-HT epoxy at 5.77 kN and the BNNT foam-HT epoxy at 4.06 kN.

The observed mechanical properties can be correlated to the microstructure of the foams in terms of their wall thickness and gap. The BNNP foam, characterized by thicker walls of 4.32 ± 0.58 μm and larger wall gaps of 100.92 ± 19.70 μm, provides a more robust structure capable of bearing higher loads. These thicker walls increase the ability of the BNNP foam to distribute and bear compressive loads. In contrast, the BNNT foam has thinner walls, measuring 0.99 ± 0.15 μm and smaller wall gaps of 27.46 ± 3.68 μm, resulting in a lower load-bearing capacity. Thinner walls lower the ability of the BNNT foam to resist both elastic and plastic deformation. The hybrid BNNT/BNNP foam, with a wall thickness of 3.04 ± 0.93 μm and wall gaps of 65.73 ± 8.64 μm, shows intermediate mechanical performance. This structural variation directly influences the foams' ability to distribute and bear mechanical loads, thereby affecting their overall mechanical behavior.

The higher maximum loads observed with foam walls aligned parallel are due to the load being applied along the walls' length, enabling more efficient load-bearing and distribution through a continuous material path. In contrast, when the walls are perpendicular to the load, the foams show reduced load-bearing capacity because the load must transfer across weaker wall interfaces, resulting in diminished mechanical strength. The foams with perpendicular walls to the loading relied on the interconnecting bridge structures to bear the compressive load, as can be observed in **Supplementary Videos 4–6**. These interconnecting bridges exhibited a spring-like behavior, facilitating long-distance stress transfer and preventing localized failure. This flexible structure prevents brittle failure by allowing the material to deform elastically rather than crack under stress.

Furthermore, this elastic deformation behavior is evident in the load-displacement curves shown in Fig. 5b. The curves demonstrate a linear and continuous relationship during both the loading and unloading phases, indicative of a stable energy absorption process. The absence of abrupt changes or irregularities in the curves suggests uniform stress

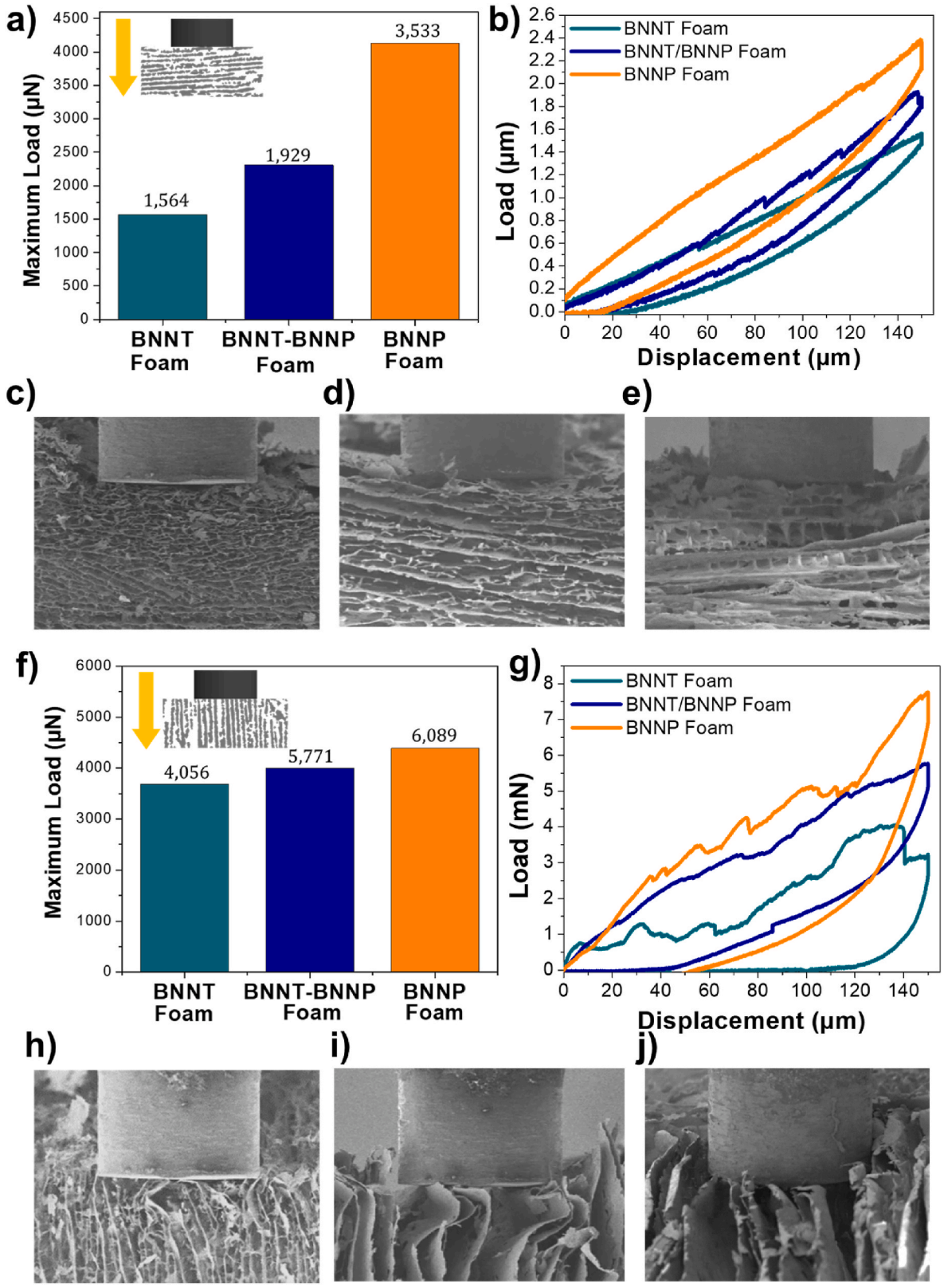

Fig. 5. Mechanical characterization of BN foams: a) maximum load and b) load-displacement curves from *in-situ* nanoindentation of BN foams in perpendicular orientation; c-e) micrographs of BNNT, BNNT/BNNP, and BNNP foams. f) Maximum load and g) load-displacement curves from *in-situ* nanoindentation of BN foams in parallel orientation; h-j) micrographs of BNNT, BNNT/BNNP, and BNNP foams.

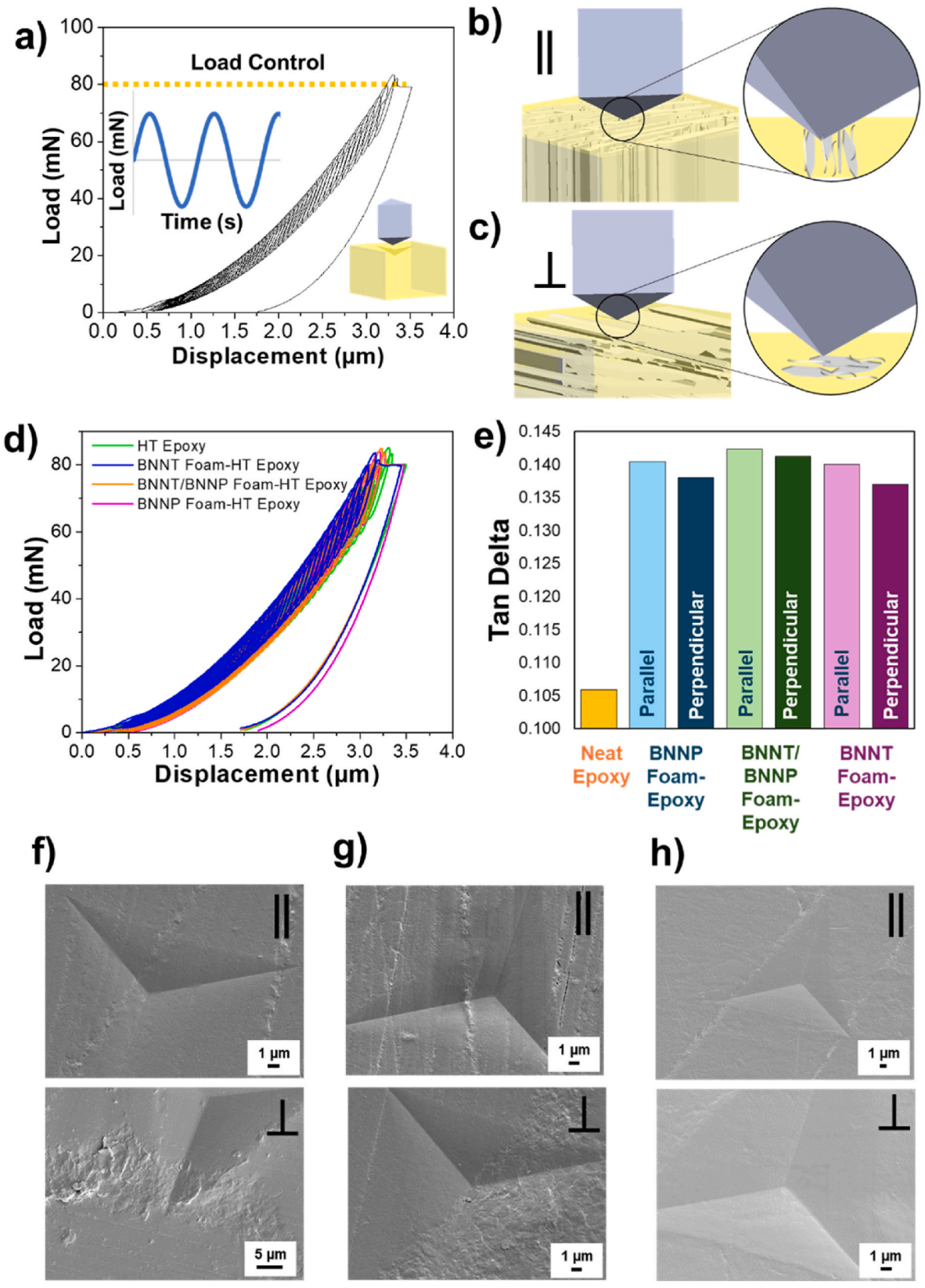

Fig. 6. Damping characterization of BN foam-HT epoxy composites: a) dynamic nanoindentation setup, b) parallel foam configuration, c) perpendicular foam configuration, d) load-displacement curves, e) tan delta values of BN foam-HT epoxy composites, and micrographs of f) BNNP foam-HT epoxy, g) BNNT/BNNP foam-HT epoxy, and h) BNNT foam-HT epoxy.

distribution and effective energy dissipation.

In contrast, the foams with walls parallel to the loading direction heavily relied on the walls to bear the compressive load, as can be observed in **Supplementary Videos 7–9**. During indentation, the energy was fully absorbed by the elastic deformation of the walls before plastic deformation occurred. This plastic deformation was reflected as inelastic buckling of the BN foam walls. The plastic deformation was transmitted along the interconnected pathways offered by the parallel wall architecture of the 3D foam. The load-displacement curves in Fig. 5g exhibit pronounced fluctuations. These fluctuations, characterized by distinct peaks and valleys in the curves, represent alternating phases of load-bearing and load release as the walls undergo sequential elastic and plastic deformation. The peaks correspond to moments of maximum stress concentration, where the material temporarily resists further deformation. At the same time, the subsequent drops or valleys reflect the onset of buckling and the redistribution of stress across the foam structure. The microstructure of the BNNT, BNNT/BNNP, and BNNP foams under indentation in the parallel orientation can be observed in Fig. 5h to j.

This complex mechanical response underscores the anisotropic nature of the material, where the parallel wall alignment contributes to a less uniform stress distribution under load. The repetitive buckling and recovery cycles captured in the load-displacement curves indicate the material's capacity to absorb and dissipate energy through successive deformation events, albeit with a reduced smoothness compared to perpendicular configurations. This behavior highlights the importance of wall orientation in determining the mechanical performance and energy dissipation characteristics of the foams. After establishing an understanding of the mechanical behavior of BN foams, the damping characteristics of BN foam-HT epoxy composites were studied. The mechanical properties of the BN foams provide a foundation for understanding their interaction with high-temperature epoxy matrix and their impact on the overall damping performance of the composites.

The BN foams infiltrated with HT epoxy were characterized using a dynamic sinusoidal mode nanoindentation test. Fig. 6a shows the nanoindentation dynamic sinusoidal mode test setup, where a controlled oscillatory load is applied to the sample to evaluate its mechanical response under dynamic conditions. Similarly to the nanoindentation tests on the BN foams, the BN foam-HT epoxy composites were characterized in both parallel and perpendicular configurations, as shown in Fig. 6b and c, respectively. The load-displacement curves of the neat HT epoxy and BN foams-HT epoxy composites can be observed in Fig. 6d. The damping behavior of the composites was characterized by *tan δ*, which is a damping factor defined as the relationship in equation (6).

$$tan\,\delta = \frac{E''}{E'} \tag{6}$$

Here, E'' is the loss modulus, and E' is the storage modulus.

Fig. 6e compares the *tan δ* values of the composites, highlighting the damping properties. Neat HT epoxy exhibited a *tan δ* of 0.106. In the parallel orientation, the composites with BNNP foam, BNNT/BNNP foam, and BNNT foam showed tan δ value improvements of 32 %, 34 %, and 32 % over neat HT epoxy, respectively. In the perpendicular orientation, the composites with BNNP foam, BNNT/BNNP foam, and BNNT foam demonstrated *tan δ* values enhancements of 30 %, 33 %, and 29 % over neat HT epoxy, respectively.

The neat HT epoxy exhibited lower damping properties than all the composites in either orientation due to the absence of the reinforcing BN structures. However, these results demonstrate that incorporating BN foams into HT epoxy significantly enhances the damping properties by 31.7 ± 1.6 %, regardless of the foam orientation or the BN nanomaterial morphology. A factor contributing to the damping behavior of the BN foam-HT epoxy composites is the inter-wall networking within the BN-lamellar foams. This interconnectivity enhances energy dissipation through mechanical friction and deformation between the walls. These inter-wall interactions improve damping efficiency by distributing mechanical energy throughout the foam structure, thereby reducing the overall amplitude of vibrations. Additionally, the presence of the elastomeric binder (SBR) contributes to the damping effect, as SBR is well known for its ability to absorb and dissipate mechanical energy. It is the synergistic interaction between the BN nanomaterials and the SBR that likely enhances the overall damping performance. This interaction facilitates greater energy absorption and dissipation compared to neat HT epoxy.

The lack of orientation-dependent differences suggests that the anisotropic damping behavior inherent to the BN foams is diminished in the composites. Similarly, the absence of significant differences between the different BN nanomaterial morphologies indicates that the specific morphology of the BN nanomaterials has a minimal impact on the damping behavior of the composites under these testing conditions. The microstructure of the indents on BNNT, BNNT/BNNP, and BNNP foam-epoxy composites in both orientations can be observed in Fig. 5f to h.

This can be attributed to the nature of the relatively low-load nanoindentation testing used to evaluate damping. At these low loads, the nanoindenter probe interaction with the composite material is rather limited to BN structural walls or individual BN nanomaterials. Consequently, most of the mechanical energy is absorbed and dissipated by the epoxy and the dispersed BN nanomaterials, with minimal contribution from the foam's anisotropic architecture or the specific BN morphology. This results in similar enhancements in damping properties irrespective of the foam orientation or the type of BN nanomaterial used.

4. Conclusions

This study underscores the potential of BN foam-HT epoxy composites as lightweight, multifunctional materials for space exploration, where neutron radiation shielding, thermal management, and mechanical damping are critical. We investigated the influence of different BN nanomaterial morphologies—1D BN nanotubes (BNNT) and 2D BN nanoplatelets (BNNP)—on the performance of these composites. Our results demonstrate that BNNT foams provide superior neutron radiation shielding, attributed to their larger surface area, which enhances neutron capture efficiency. Hybrid BNNT/BNNP foams, however, outperformed in terms of thermal conductivity, highlighting the advantages of combining 1D and 2D morphologies to create more efficient heat transfer pathways. Mechanical testing showed that BNNP foams were the most resilient under nanoindentation, suggesting that the 2D structure contributes to superior load-bearing capacity. Additionally, the BN foams significantly enhanced the damping properties of the HT epoxy, regardless of BN morphology or foam orientation. This improvement in damping behavior is crucial for materials exposed to harsh mechanical environments, such as those encountered in space. The combination of neutron shielding, thermal management, and mechanical damping makes BN foam-HT epoxy composites highly promising for use in demanding environments, particularly in space exploration. The findings of this study suggest that by tailoring the BN nanomaterial composition and morphology, it is possible to optimize these composites further to meet specific application needs. The ability to enhance multiple critical properties simultaneously positions these composites as strong candidates for future aerospace and advanced engineering applications.

CRediT authorship contribution statement

Kazue Orikasa: Writing – original draft, Validation, Methodology, Investigation, Formal analysis, Data curation. **Luiza Benedetti:** Methodology, Investigation. **Sang-Hyon Chu:** Methodology, Investigation, Data curation. **Tyler Dolmetsch:** Methodology, Investigation, Formal analysis. **Alberto Jimenez:** Methodology, Investigation, Formal analysis. **Denny John:** Methodology, Investigation. **Teagan Smith:**

Methodology, Investigation. **Tony Thomas:** Supervision, Methodology, Investigation. **Benjamin Boesl:** Supervision. **Cheol Park:** Supervision, Resources, Project administration, Methodology, Investigation, Data curation. **Arvind Agarwal:** Writing – review & editing, Supervision, Resources, Project administration, Methodology, Investigation, Funding acquisition, Conceptualization.

Data availability statement

The authors declare that the data supporting the findings are available within the paper and its supplementary information.

Inclusion and ethics

The authors affirm that the current study adheres to inclusion and ethics criteria.

Funding sources

The presented work is supported by the National Aeronautics and Space Administration (NASA) Space Technology Graduate Research Opportunities (NSTGRO) [grant number 80NSSC22K1190] and the Air Force Office of Scientific Research (AFOSR) [grant number FA9550-21-1-0460].

Declaration of competing interest

The authors declare that they have no known competing financial interests or personal relationships that could have appeared to influence the work reported in this paper.

Acknowledgements

The authors would like to acknowledge the support of the Plasma Forming Laboratory (PFL) members and the Advanced Materials Engineering Research Institute (AMERI) at Florida International University (FIU) for providing the research facilities used in this study.

Appendix A. Supplementary data

Supplementary data to this article can be found online at https://doi.org/10.1016/j.compscitech.2024.110995.

Data availability

Data will be made available on request.

References

[1] S.A. Thibeault, J.H. Kang, G. Sauti, C. Park, C.C. Fay, G.C. King, Nanomaterials for radiation shielding, MRS Bull. 40 (10) (2015 Oct) 836–841.
[2] S. Zhang, R.F. Wimmer-Schweingruber, J. Yu, C. Wang, Q. Fu, Y. Zou, et al., First measurements of the radiation dose on the lunar surface, Sci. Adv. 39 (2020 Sep 25) 6, eaaz1334.
[3] R. Barber, Q. Nguyen, J. Brockman, J. Gahl, J. Kwon, Thermal neutron transmutation doping of GaN semiconductors, Sci. Rep. 10 (1) (2020 Oct 1) 16295.
[4] J. Prinzie, F.M. Simanjuntak, P. Leroux, T. Prodromakis, Low-power electronic technologies for harsh radiation environments, Nat Electron 4 (4) (2021 Apr 26) 243–253.
[5] R.S. Barnes, Embrittlement of stainless steels and nickel-based alloys at high temperature induced by neutron radiation, Nature 206 (4991) (1965 Jun) 1307–1310.
[6] B. Kombaiah, Y. Zhou, K. Jin, A. Manzoor, J.D. Poplawsky, J.A. Aguiar, et al., Nanoprecipitates to enhance radiation tolerance in high-entropy alloys, ACS Appl. Mater. Interfaces 15 (3) (2023 Jan 25) 3912–3924.
[7] C. Tan, Z. Dong, Y. Li, H. Zhao, X. Huang, Z. Zhou, et al., A high performance wearable strain sensor with advanced thermal management for motion monitoring, Nat. Commun. 11 (1) (2020 Dec) 3530.
[8] H. Song, J. Liu, B. Liu, J. Wu, H.M. Cheng, F. Kang, Two-dimensional materials for thermal management applications, Joule 2 (3) (2018 Mar) 442–463.
[9] W. Liu, Y. Gao, L. Zhang, T. Zou, M. Yu, T. Zheng, Flight test results for microgravity active vibration isolation system on-board Chinese Space Station, Npj Microgravity 10 (1) (2024 Feb 19) 19.
[10] C. Bifa, J. Liao, J. Yan, H. Li, C. Huang, A multi-point decentralized control for mitigating vibration of flexible space structures using reaction wheel actuators, Sci. Rep. 14 (1) (2024 May 6) 10326.
[11] X. Chen, C.M. Dmuchowski, C. Park, C.C. Fay, C. Ke, Quantitative characterization of structural and mechanical properties of boron nitride nanotubes in high temperature environments, Sci. Rep. 7 (1) (2017 Dec) 11388.
[12] A.L. Tiano, C. Park, J.W. Lee, H.H. Luong, L.J. Gibbons, S.H. Chu, et al., Boron nitride nanotube: synthesis and applications, in: V.K. Varadan (Ed.), San Diego, California, USA, 2014, in: http://proceedings.spiedigitallibrary.org/proceeding.aspx?doi=10.1117/12.2045396.
[13] Y. Jia, T.D. Ajayi, J. Morales, M.A.R. Chowdhury, G. Sauti, S. Chu, et al., Thermal properties of polymer-derived ceramic reinforced with boron nitride nanotubes, J. Am. Ceram. Soc. 102 (12) (2019 Dec) 7584–7593.
[14] R. Agrawal, A. Nieto, H. Chen, M. Mora, A. Agarwal, Nanoscale damping characteristics of boron nitride nanotubes and carbon nanotubes reinforced polymer composites, ACS Appl. Mater. Interfaces 5 (22) (2013 Nov 27) 12052–12057.
[15] A. Falin, Q. Cai, E.J.G. Santos, D. Scullion, D. Qian, R. Zhang, et al., Mechanical properties of atomically thin boron nitride and the role of interlayer interactions, Nat. Commun. 8 (1) (2017 Aug) 15815.
[16] K. Orikasa, C. Park, S.H. Chu, C. Lum, T. Thomas, T. Dolmetsch, et al., Foam with direction: unraveling the anisotropic radiation shielding properties of 2D boron nitride nanoplatelet foams, Npj 2D Mater Appl. 8 (1) (2024 Feb 26) 13.
[17] N.D. Badgayan, S.K. Sahu, S. Samanta, P.S. Rama Sreekanth, Assessment of nanoscopic dynamic mechanical properties and B-C-N triad effect on MWCNT/h-BNNP nanofillers reinforced HDPE hybrid composite using oscillatory nanoindentation: an insight into medical applications, J. Mech. Behav. Biomed. Mater. 80 (2018 Apr) 180–188.
[18] I.A. Kinloch, J. Suhr, J. Lou, R.J. Young, P.M. Ajayan, Composites with carbon nanotubes and graphene: an outlook, Science 362 (6414) (2018 Nov 2) 547–553.
[19] A. Idowu, B. Boesl, A. Agarwal, 3D graphene foam-reinforced polymer composites – a review, Carbon 135 (2018 Aug) 52–71.
[20] T. Thomas, A. Agarwal, A. Facile, Scalable approach in the fabrication of tailored 3D graphene foam via freeze drying, Materials 14 (4) (2021 Feb 11) 864.
[21] K. Orikasa, T. Dolmetsch, L. Lou, T. Thomas, B. Boesl, A. Agarwal, Orientation-dependent thermal and mechanical properties of 2D boron nitride nanoplatelet foams via freeze-drying, ACS Appl. Nano Mater. 6 (20) (2023 Oct 27) 19048–19060.
[22] B.N.N.T. Nanotubes. https://www.bnnt.com/nanotubes, 2024.
[23] V. Guerra, C. Wan, T. McNally, Thermal conductivity of 2D nano-structured boron nitride (BN) and its composites with polymers, Prog. Mater. Sci. 100 (2019 Feb) 170–186.
[24] X. Wang, A. Pakdel, J. Zhang, Q. Weng, T. Zhai, C. Zhi, et al., Large-surface-area BN nanosheets and their utilization in polymeric composites with improved thermal and dielectric properties, Nanoscale Res. Lett. 7 (2012) 1–7.
[25] J.P. Holman, Heat Transfer, tenth ed., 2010. McGraw-Hill Education.